ELSEVIER

Nuclear Instruments and Methods in Physics Research B 133 (1997) 134–144

NIM B
Beam Interactions with Materials & Atoms

A review of the current status of XAFS spectroscopy

E. Daryl Crozier

Physics Department, Simon Fraser University, Burnaby, B.C., Canada V5A 1S6

Abstract

The major experimental and theoretical problems in XAFS spectroscopy have been identified for many years, but now have solutions. The analysis of first shell Gaussian distributions have become routine. The analysis of systems with anharmonic potentials or asymmetric distributions has progressed to the point where effective pair potentials and thermal expansion coefficients of bonds can be obtained. This review focuses on recent advances in extracting the XAFS interference function from the absorption background, developing theoretical standards for amplitudes and phase shifts, treating multiple scattering (MS) and analysing liquids. It is expected that analysis of solids to 6–8 Å will become routine. While unconstrained curve-fitting is generally not possible, constrained curve-fitting and simulations can clarify the structure as indicated with examples. Further treatment of the dynamical motion of atoms involved in the MS paths is required. Correlated vibrational motion may lead to an error in bond angles. The loss of low k-data remains a problem in determining partial pair distributions functions in liquids, but progress has been made. © 1997 Elsevier Science B.V.

1. Introduction

Synchrotron radiation has permitted rapid development of XAFS, the spectroscopy of the fine structure in the X-ray absorption coefficient above an absorption edge. XAFS encompasses both the extended (EXAFS) and near edge regimes, providing local structural information: interatomic distances, number and identity of coordinating atoms, information about the correlated motion between the absorbing atom and its neighbour, and in some circumstances, bond angles.

XAFS provides the partial pair distribution functions with high spatial resolution. Long range order is not required, so that the local structure of liquids, glasses and amorphous solids can be determined using the same analysis procedures as for crystalline materials. The concentration of the absorbing species can be as low as parts per million. An XAFS spectrum can be measured by a variety of detection methods relaxing some constraints on sample preparation, increasing the ease of application to the diverse materials encountered in materials science.

Experimental details and the theoretical framework of XAFS have been reviewed intensively [1–4], including general principles of analysis [5]. For nearest neighbours, procedures are well established, providing radial distances, R_i and coordination number with high accuracy for strongly bonded atom pairs for which the effective two-body potential is harmonic. Anharmonic potentials or asymmetric distributions were once considered to pose a limitation, but with present analysis methods it is now possible to go beyond the simple extraction of static structural parameters and to

S0168-583X/97/$17.00 © 1997 Elsevier Science B.V. All rights reserved.
PII S0168-583X(97)00471-0

determine effective pair potentials and thermal expansion coefficients of bonds. These developments have been reviewed recently [6]. Beyond the first nearest neighbour multiple scattering (MS) must be included. The very rapid growth of the number of scattering paths with distance greatly complicates analysis. However, curved wave MS theory has developed to the point where unknown structures can be simulated out to ~6 Å with sufficient accuracy to distinguish between models.

This paper focuses on the remaining major problems in XAFS: extraction of the XAFS interference function $\chi(k)$ from the absorption background, developing theoretical standards for scattering amplitudes and phase shifts, an efficient treatment of MS, and the analysis of liquids. It begins with the XAFS equations suitable for Gaussian and asymmetric distributions in the single scattering (SS) approximation and then includes MS. Recent developments in background removal and the status of theoretical amplitude and phase shifts are given in Section 3. Section 4 contains examples of MS and the analysis of liquids is reviewed in Section 5. Conclusions are given in Section 6.

2. The XAFS equations

The structural information is contained in the XAFS interference function $\chi(k)$, the normalized oscillatory part of the X-ray absorption coefficient $\mu(E)$, and can be written for the K-edge [1] of a monatomic system in the SS curved wave approximation as

$$\chi(k) = S_0^2 \int \mathrm{d}r\, P(r) \frac{f(k,r)}{k} \frac{\mathrm{e}^{-2r/\lambda}}{r^2} \times \sin(2kr + \delta(k,r)), \quad (1)$$

where k is the wave vector of the photoelectron. The scattering of the photoelectron from the neighbouring atoms is specified by the magnitude of the backscattering amplitude $f(k,r)$ and the phase shift $\delta(k,r) = 2\delta_c(k) + \delta_b(k,r)$, where $\delta_c(k)$ is the phase shift for the central atom and $\delta_b(k,r)$ is for the backscatterer. The r-dependence of the scattering is small, but measurably different between first and second nearest neighbours. The lifetime of the final state of the photoelectron is included phenomenologically by $\mathrm{e}^{-2r/\lambda}$ with the mean free path λ. S_0^2 is a slowly varying function of k describing the reduction of $\chi(k)$ due to multiple electron effects.

The probability of finding an atom at distance r from the X-ray absorbing atom is specified by $P(r)$. The "standard" XAFS equation is obtained by assuming a Gaussian distribution of atoms about the absorbing atom given by $P(r) = \exp(-(r-R_j)^2/2\sigma_j^2)/\sqrt{2\pi\sigma_j^2}$, where R_j is the average distance between the absorber and jth backscatterer and σ_j^2 the mean square relative displacement between the absorber and scattering atoms. In the small disorder limit [7,8]

$$\chi(k) = \sum_j S_0^2 N_j \frac{\mathrm{e}^{-2k^2\sigma_j^2}}{kR_j^2} \mathrm{e}^{-2R_j/\lambda} f(k,R_j) \times \sin\left[2k(R_j - \Delta_j) + \delta_j(k,R_j)\right], \quad (2)$$

where the summation is over shells of radius R_j with coordination number N_j. The phase correction term $\Delta_j = (2\sigma_j^2/R_j)(1 + R_j/\lambda)$ arises by correctly including the contribution of $\mathrm{e}^{-2r/\lambda}/r^2$ to the integral [7]. This is normally a small correction: in Cu metal at room temperature it is ~0.007 Å. For anisotropic samples the polarization dependence is included in the SS approximation by replacing N_j by $N_j^* = 3\sum_j^{N_j} \cos^2\alpha_j$, where the summation is over the number of atoms in the jth shell and α_j the angle between the electric vector of the X-ray wave and the vector direction from the absorber to the backscatterer [9,10].

For systems for which Eq. (2) is applicable, with careful data analysis, it is possible for the nearest neighbour shell to determine R_j to an accuracy of ±0.02–±0.003 Å, and N_j and σ_j^2 to an accuracy of ±10–±2%. It is also possible, if the k-space

[1] In the dipole approximation $\mu(E)$ is determined by the selection rule $\Delta\ell = \pm 1$. For K- or L_1-edges transitions from 1s or 2s initial states to final states with p symmetry are involved. For L_2- or L_3- edges transitions from $2p_{1/2}$ or $2p_{3/2}$ initial states to final states with s and p symmetry must be included. For unoriented samples, transitions to states with s symmetry are usually negligible, but they must be included for oriented single crystals and surfaces which are intrinsically anisotropic.

range of data is sufficient, to distinguish nearest neighbours which differ in atomic number by more than ~5.

It should be noted that diffraction and XAFS are complementary, rather than competing, techniques. XAFS probes short range order and not long range order. For example, in the random solid solution $Ga_{1-x}In_xAs$, it was shown by XAFS that Ga–As, In–As nearest neighbour distances retain essentially the same values as in the pure compounds and do not have the average positions calculated from (X-ray) diffraction lattice constants and the assumption of Vegard's law [11].

The pair distribution function is obtained by XAFS with a higher spatial resolution than normally achieved with diffraction. In XAFS it is limited by the finite range of the data according to $\Delta R = \pi/2\Delta k$, where $\Delta k = k_{max} - k_{min}$. In diffraction experiments the spatial resolution in the pair distribution function is determined by the momentum transfer calculated from $q = 2k \sin \theta$, where 2θ is the angle through which the incident photon, electron or neutron of momentum $\hbar k$ is elastically scattered and is twice the photoelectron momentum $\hbar k$. Generally, the upper limit is higher with XAFS. In disordered solids or liquids k_{max} is ~15 Å^{-1}, but in ordered solids where the backscattering atoms have high atomic number the upper limit k_{max} is ~25 Å^{-1}. In liquids and amorphous solids [8], with conventional diffraction techniques, typically $q_{max} \sim 12$ Å^{-1} (corresponding to k_{max} ~6 Å^{-1} in XAFS), although with the time-of-flight neutron scattering method $q_{max} \sim 40$ Å^{-1} is possible. The high resolution of XAFS permitted a beat frequency at 12 Å^{-1} in the Cu K-edge $\chi(k)$ of $YBa_2Cu_3O_{7-\delta}$ to be identified with a two site distribution for the Cu(1)–O(4) axial oxygen [12]. The temperature dependence of the distribution was related to the mechanism of high T_C superconductivity (although subsequent XAFS studies have found the presence of the two site distribution to be sample-dependent [13,14]).

In diffraction experiments the lower q-limit q_{min} is ~0.5 Å^{-1} whereas, until recently, difficulty in extracting $\chi(k)$ from the absorption background and uncertainties in $S_0^2 f(k,r)\exp(-2r/\lambda)$ have limited many XAFS analyses to $k_{min} \sim 3$ Å^{-1}. In a diffraction experiment this would be equivalent to discarding data for $q_{min} < 6$ Å^{-1} in the structure factor $S(q)$. [2] If the pair distribution function $P(r)$ is Gaussian, the loss of low k-data does not affect the accuracy of the structural parameters obtainable with the standard XAFS equation.

In the classical limit the pair distribution function is related to the effective two-body potential $U(r)$ by

$$P(r) = e^{-U(r)/kT} \Big/ \int dr\, e^{-U(r)/kT}. \tag{3}$$

For a harmonic potential $U(r) = \gamma(r - R_j)^2/2$ and $P(r)$ is a Gaussian with $\sigma^2 = kT/\gamma$, where γ is the force constant. This is a good approximation if the temperature of measurement is less than the Einstein or Debye characteristic temperatures, as for example, in strongly covalent systems at room temperature. However, in all systems with increasing temperature anharmonic contributions to the vibrational displacements of atoms can no longer be neglected and $P(r)$ becomes asymmetric. $P(r)$ may also be asymmetric due to static disorder. A Gaussian may be inappropriate if σ_i^2 exceeds 0.015 Å^2 (Fig. 9.6 of Ref. [8]). The incorrect assumption of a Gaussian yields incorrect structural parameters: interatomic distances and coordination numbers are too small [7,8]. For example in the weaker "metallic" bonding of Cu, the apparent contraction is ~0.02 Å in the nearest neighbour distance at room temperature and as the melting point is approached, the coordination number can be too small by a factor of 2 [8].

When the asymmetry is small, or the disorder is low to moderate, expanding Eq. (1) in cumulants to fourth order gives [7]:

$$k\chi(k) = A(k) \sin \Phi(k), \tag{4}$$

$$A(k) = S_0^2 f(k,R) N \frac{e^{-2R/\lambda}}{R^2} e^{-2C_2k^2} e^{(2/3)C_4k^4},$$

$$\Phi(k) = 2k\left[R - \frac{2C_2}{R}(1 + R/\lambda)\right] - 4/3C_3k^3 + \delta(k).$$

[2] In liquid Gallium this would omit the first two strong oscillations in $S(q)$. See Fig. 9.23 of Ref. [8].

When cumulants C_n higher than two are negligible, Eq. (5) reduces to Eq. (2) with $C_2 = \sigma^2$. The strengths and limitations of cumulants have been determined in the extensive studies by Dalba et al. [15] on silver iodide. Silver iodide undergoes a first order solid–solid phase transition at 420 K to the superionic state where the cations become mobile. Below the transition the cumulant expansion provides a model independent method of obtaining $P(r)$, but above the transition the excluded volume model [1] of Hayes and Boyce is necessary.

The effective pair potential $U(r)$ can be obtained by inverting Eq. (3). For weakly anharmonic systems, $U(r)$ can be expanded in a power series and from the temperature dependence of the cumulants the potential coefficients can be extracted as reviewed in Ref. [16]. One important application has been to establish that enhanced harmonicity is a general surface-related property [16,17].

Cumulants give more accurate coefficients of thermal expansion, α, than can be obtained by direct measurement of the n–n distance with the temperature [16]. However, in AgI the thermal expansion coefficient measured by XAFS is significantly larger than measured by diffraction. This effect is of general origin. It is caused by vibrational motion normal to the n–n bond direction contributing to the XAFS distance and the mean square relative displacement σ_i^2 [15]. This effect should be considered in future measurements of not only α, but also in determining anisotropy in σ_i^2 and $U(r)$.

References to other analysis methods such as the splice method, Monte Carlo simulations, reverse Monte Carlo, and molecular dynamics are given in a review of asymmetric distribution functions [6].

For distances greater than the first nearest neighbour distance R_1, although SS is usually dominant, MS must be included [18]. The scattering amplitude $f(\beta,k)$ is a strong function of the scattering angle β, Fig. 1. In the forward scattering direction, $\beta = 0°$, the scattering amplitude can be substantially larger than for the backscatter direction $\beta = 180°$. When two or more scattering atoms are collinear the photoelectron is "focused" in the forward direction such as along the face-centered or body-centered diagonals in fcc and bcc metals,

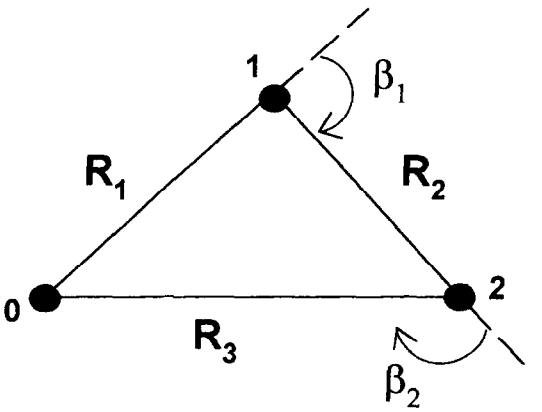

Fig. 1. Arrangements of atoms for which MS affects the XAFS determination of the distance R_3. The absorbing atom is labelled 0 and the scatterers are 1 and 2. The photoelectron travels the path Γ, 0–1–2–0 or 0–2–1–0, with an effective path length $2R = R_1 + R_2 + R_3$. Thermal motion may change the MS especially if the angle β_1 is near zero.

producing the well-known increase in the amplitude of the fourth and fifth shells, respectively. At intermediate angles, $f(\beta,k)$ is reduced relative to forward and backscattering, but triangular and higher order paths can be important in high symmetry sites due to the degeneracy in the number of equivalent paths. A full high order MS calculation is precluded, in general, by the rapid increase in the number of paths. For example, in Cu for $R \leqslant 8.5$ Å there are $\sim 4.3 \times 10^5$ distinct paths [19]. Full MS calculations have been done on clusters of atoms (with the ICXANES code [20,21]) but quickly become CPU limited as the size of the cluster and highest k-value are increased.

Rehr et al. [19] have shown that curved wave and MS effects can be expressed in a form analogous to the standard XAFS equation for each path Γ

$$\chi^{\Gamma}(k) = \sum_{\Gamma} \frac{S_0^2}{kR^2} |f_{\mathrm{eff}}^{\Gamma}(k)| \mathrm{e}^{-2R/\lambda(k)} \mathrm{e}^{-2\sigma_i^2 k^2} \times \sin(2kR + \Phi^{\Gamma}(k) + 2\delta_{\mathrm{C}}(k)). \quad (5)$$

Here $f_{\mathrm{eff}}^{\Gamma}(k)$ is the effective scattering amplitude for the path Γ, $\Phi^{\Gamma}(k)$ the net scattering phase shift, and $2R$ the effective length of path Γ illustrated in Fig. 1 for a triangular path. The correlated

motion of the atoms is included via the path-dependent Debye–Waller factor $\exp(-2k^2\sigma_\Gamma^2)$, where $\sigma_\Gamma^2 = \langle(\delta R)^2\rangle$ is the mean square variation in R for path Γ. Rehr et al. have developed an efficient path-enumeration algorithm which converges to full MS accuracy in extended systems, without the need for symmetry or matrix diagonalizations. In their computer code FEFF5, MS paths Γ are presorted, retaining only those that are significant. For example, in fcc Cu and Pt agreement of theory to within a few percent of low temperature data was obtained to 8 Å with ~100 paths with SS, focusing and triangular paths being the most important. The path-dependent Debye–Waller factor was approximated by the correlated Debye model or by fitting the Debye–Waller factors independently. The treatment of the MS Debye–Waller factor needs more attention, particularly for nonmetals, but other aspects of the MS XAFS are generally considered to be solved. The biggest remaining uncertainties in the FEFF code are the self-energy near threshold, the magnitude and energy dependence of S_0^2 and the atomic background absorption [19].

The effect of MS on the polarization dependence of surface XAFS has been considered using the full curved wave theory, including all orders of MS up to five [22]. The FEFF code has been extended in FEFF6 to include general elliptical polarization so that polarized MS XAFS calculations can now be done on arbitrary materials [19].

3. Background removal and theoretical scattering standards

The oscillatory interference function $\chi(k)$ must be removed from the background absorption. Higher order polynomials or cubic splines are usually satisfactory approximations to the low frequency component of the background [5,23] for k greater than about 3.5 $Å^{-1}$ but are problematic for smaller k. Yet it is important to extract $\chi(k)$ to lower k-values to maximize the spatial resolution, to include more of the MS contributions whose amplitudes tend to be larger at small k and negligible for $k > 6\,Å^{-1}$, to better analyse asymmetric distributions by having an improved extrapolation to $k = 0$, and to permit improvements to theoretical calculations of $\delta(k,r)$ and $S_0^2 f(k,r)\exp(-2r/\lambda)$. Recent background removal schemes have been successful in isolating steps and oscillations due to multi-electron excitations and removing atomic XAFS. An iterative scheme has been developed in which the initial background fit is refined by removing a $\chi(k)$ fit to the first few neighbours [24–26]. An algorithm, AUTOBK, uses cubic splines but places the nodes at equal k-space sampling intervals π/R_{min}, where R_{min} is the frequency below which the XAFS content can be neglected [27]. With a different background removal scheme [28] it has been shown when double electron excitation effects are correctly included in the atomic background that S_0^2 approaches 1.0 [28–31]. With these different approaches extracting experimental $\chi(k)$ that are reliable to $k \approx 2\,Å^{-1}$ are now feasible.

Historically, the most accurate data analysis with Eq. (2), used reference compounds of known structure to transfer S_0^2, $f_j(k,R_j)$, $\delta(k,R_j)$, and λ to the unknown system. But with advances in the theory, convergence of different theoretical groups in their numerical results and the availability of computer codes for the calculation of amplitudes and phase shifts, the need for data on reference compounds is reduced. For example, a comparison of 30 isolated pair standards [32] with FEFF5 found errors in the n–n distance to be typically 0.005 Å. For high atomic number backscatterers ($Z > 40$) differences were sometimes found for $k < 7\,Å^{-1}$ and experimental standards provided better fits to the data. S_0^2 was also found to be somewhat dependent on the local chemical environment surrounding the absorbing atom.

4. Multiple scattering examples

With present day computing codes, MS is easily included in data analysis. This will now be illustrated using FEFF6 [19] and an over-simplified treatment of Cr metal for which MS should be included in the first shell analysis. The strength of the MS depends upon the atomic numbers of the scatterers and, for example, is not important in the first shell analysis of bcc Fe which has almost

the same lattice constant as Cr. At room temperature Cr has the lattice constant $a = 2.8839$Å, $R_1 = \sqrt{3}a/2 = 2.4975$ Å, $R_2 = a$, $N_1 = 8$, and $N_2 = 6$. As shown in Fig. 2, R_1 and R_2 cannot be separated by Fourier filtering. Using the standard XAFS Eq. (3) to fit the inverse transform of the main peak in the transform to a 2-shell model gives a visually good fit, Fig. 3, when N_2 is constrained to the crystal value $N_2 = 0.75N_1$ and $S_0^2 N_1$ is an adjustable parameter. Defining the difference Δ as the fit value minus the crystal value, then the values $\Delta R_1 = 0.0035$ Å and $\Delta R_2 = -0.019$ Å seem to be acceptable. But it is not possible with just one adjustable E_0 while constraining $N_2 = 0.75N_1$ to reduce ΔR_2 and still keep a reasonable value of $S_0^2 N_1$. The residual $\chi(k)$, obtained by subtracting the 2-shell fit result from the filtered $\chi(k)$, has a high frequency component similar to the contribution from triangular MS paths, Fig. 3. In the bcc structure there are a total of 72 triangular paths involving R_1 and R_2 with the same effective XAFS

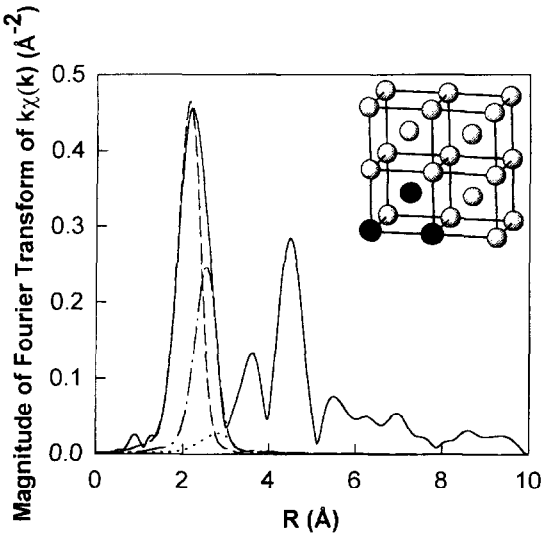

Fig. 2. The magnitude of the Fourier transform of $k\ \chi(k)$ of Cr metal (solid line) at room temperature. Overlaid are the contributions of first neighbours, corner to body-centre (dash) distance R_1, second n–n, corner to corner (dot-dash) distance R_2, and the triangular MS paths (dot) R_{MS}, involving the corner and body-centre atoms of the bcc structure, type 112 and 121 where "1" denotes a path leg of length R_1 and "2" a leg of length R_2. The transform of $k\ \chi(k)$ was taken over the range $1.85 < k < 13.7$ Å^{-1} with a 10% Gaussian window.

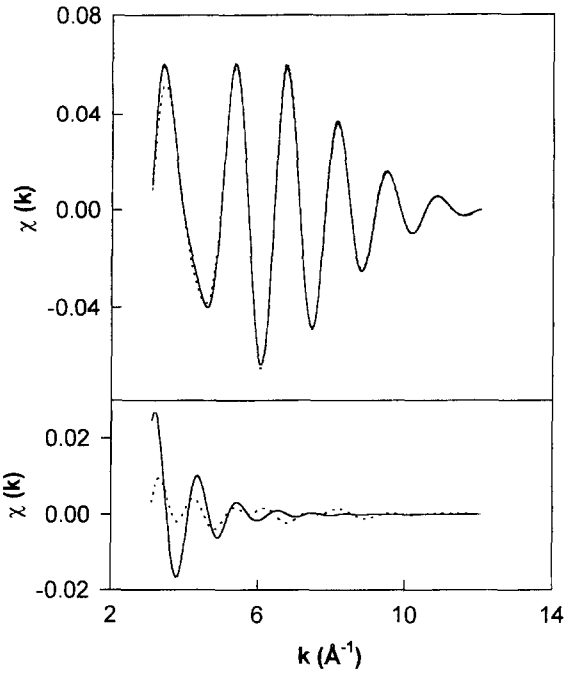

Fig. 3. The MS contributions to the first shell $\chi(k)$ of Cr metal. Upper panel: The Fourier filtered data (solid line) and its fit with (long dashes) and without (dots) triangular MS contributions. The filtered $\chi(k)$ was obtained by taking the inverse transform over the range $0.9 < R < 3.1$ Å in Fig. 2. Lower panel: The residual $\chi(k)$, (filtered data – fit without MS) (dots), and $\chi(k)_{MS}$ for the triangular MS paths (solid line) calculated with FEFF6.

distance $R_{MS} = R_1 + 0.5R_2$, 48 paths are of the type 112 and 24 are of the type 121 using the notation "1" to denote a path of length of R_1 and "2" for the length R_2 [18,19]. The phase shift $\Phi^{\Gamma}(k)$ must account for scattering from two atoms and is large, downshifting the peak associated with R_{MS} from 3.94 to ~3 Å. The scattering amplitude, $f(k,\beta)$, for angles not close to 0° or 180° is small and when the Debye–Waller factors $e^{-2k^2\sigma^2}$ for the three atoms are included, the total MS contribution to the first peak in the magnitude of the transform, Fig. 2, is characteristically small. In k-space, $\chi(k)_{MS}$, the sum of the MS triangular paths, is negligible for $k > 6$ Å, Fig. 4, but at low k it is approximately in-phase with the contribution to $\chi(k)$ of R_2. As a consequence, if the triangular paths are omitted from the fitting, as in the simple 2-shell fit, then the apparent coordination number

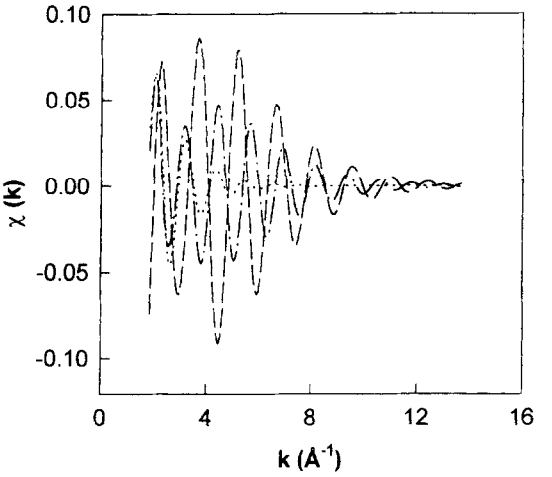

Fig. 4. The contributions to $\chi(k)$ in Cr from neighbours at R_1 (dashes), R_2 (dash-dots) and from the atoms along the MS path of length R_{MS} (dots).

for N_2 must increase and a fit constrained to $N_2 = 0.75\ N_1$ will have increased errors in R_1 and R_2. But when they are included using Eq. (5) the fit to the filtered $\chi(k)$ "snaps-into" the bcc structure and is indistinguishable from the data on the scale of Fig. 3. The fit statistic chi-squared (Eq. (2) of Ref. [33]), the residual sum of squares χ^2_ν, is reduced by a factor of 6 relative to the χ^2_ν for the 2-shell fit. The differences ΔR_1 and ΔR_2 both equal +0.002 Å, and $N_1 = 8$, $S_0^2 = 0.83$ when N_2 is constrained to equal 0.75 N_1. Comparable results are obtained fitting the same two models in R-space with the same R-space window.

The fitting presented for Cr is not intended to be a comprehensive discussion of MS. Indeed, the inclusion of the triangular MS paths in our first shell fit to Cr is inadequate. The choice of $R_{max} = 3.0$ Å neglects higher frequency components representing about 25% of the total area under the magnitude of the transform of $k\chi(k)_{MS}$. But the simplified treatment does show that the state of XAFS analysis has reached the point where one should try to determine if small residuals in k-space (or R-space) fits have a structural origin. Since programs such as FEFF6 have become available, MS refinements in XAFS analysis have become easier to include and in solids distances out to 6–8 Å should be considered routinely. Detailed discussions of MS have been given for fits including MS to 8 Å in fcc Cu, fcc Pt and hcp Cd [19] and to 10 Å in alkali halides [34]. However, in crystals having larger unit cells such as the high T_C superconductor $Tl_2Ba_2CuO_y$, it remains difficult to make a detailed fit to experimental data for $R > 4$ Å [35]. Polarization-dependent XAFS can be used to clarify specific features such as the possible existence of a double oxygen O(4) site in the axial Cu(2)–O(4) bond in the high T_C superconductor $YBa_2Cu_3O_{7-\delta}$ [13,14].

Much stronger MS contributions occur in the focusing effect for which ReO_3 provides a good example. ReO_3 has the perovskite ABO_3 structure with the A sites vacant (simple cubic with Re in the body-centre position, O in the face-centre positions and the corners vacant). At zero pressure the Re–O–Re atoms form a linear chain and the Re–Re peak in the Fourier transform is larger than the nearest neighbour Re–O peak, Fig. 5. At 5 kbar the ReO_3 octahedra begin rotations about the 1 1 1-type axes. The Re–O–Re bridging angle, β_1 in Fig. 1, increases from zero and due to the strong

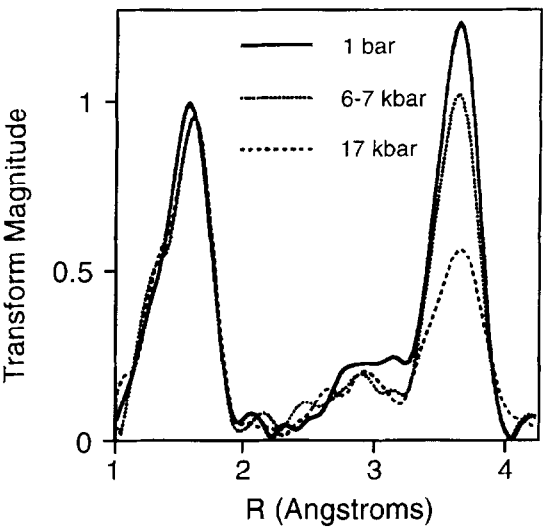

Fig. 5. Magnitude of the Fourier transform of $k^2\ \chi(k)$ for ReO_3 for three pressures. The window function for the transforms was Gaussian, symmetrically placed between 2 and 19 Å^{-1}. (Fig. 1 of Ref. [36]). The Re–Re peak at 3.5 Å is enhanced by the focusing effect along the Re–O–Re chain involving the double scattering path 0–1–2–0 and the triple scattering path 0–1–2–1–0 of Fig. 1.

decrease of $f(\beta,k)$ with β there is a dramatic decrease in the height of the Re–Re peak [36,37]. This sensitivity to β_1 provides a method of determining bond angles in chemical compounds [38]. However, dynamic fluctuations in bond angles due to thermal motion must be considered when $\beta_1 < 20°$ [39], the effect on the k-dependence of the amplitude of $\chi(k)$ cannot be described, in general, with an exponential decay of the form $\exp(-2k^2\sigma^2)$. The path-dependent Debye–Waller factor cannot be approximated by the simple Debye model used in metals. Houser confirmed that when the dynamic displacement of the centre atom is symmetric about the linear line of atoms, the XAFS is identical to the case when the central atom is statically displaced by the rms fluctuation in bond angles [36]. Thus, using FEFF5 to fit the ReO_3 data, the value of β_1 in the Re–O–Re bridge was set at a static value of 8° and not 0° at 1 bar. The rotation angles subsequently found at higher pressure were then in agreement with neutron diffraction data [36]. We conclude that if the dynamical fluctuation in bond angles is not included correctly, errors of the order of 10° may occur, for example, in μ-oxo metal bridging angles found in proteins and there may be correspondingly larger than normal errors in the metal–metal distance R_3. The contribution of bending moments to octahedral Pt–halogen complexes has been studied [40].

Rotation of the oxygen octahedra are involved in antiferrodistortive phase transitions (APT) in perovskite crystals ABO_3. The transitions have normally been considered to be purely displacive. However, due to the sensitivity of the MS paths to the octahedra rotation, XAFS has been able to show that the antiferrodistortive transition in $Na_xK_{1-x}TaO_3$ also involves orientational order–disorder contributions [41]. The MS XAFS has also shown that order–disorder is present in the displacive ferroelectric transition in $PbTiO_3$ [42]. In $Pb_{1-x}Ge_xTe$ the high spatial resolution of XAFS and just a first shell analysis, where MS is not relevant, was sufficient to enable Islam and Bunker [43] to show that the ferroelectric transition was a simultaneously order–disorder and displacive transition.

The MS has been important in showing that the crystalline structure of mixed ionic salts, of the form $RbBr_xCl_{1-x}$, buckles to accommodate the mismatch in atomic size [44,45]. Rb and Br K-edge XAFS show that the atoms deviate from a perfect periodic structure, the average interatomic distances as determined from the first XAFS shell analysis, weighted by concentration, being greater than the lattice spacing measured by X-ray diffraction. This means that linear chains of the type Rb–Cl (or Br) –Rb must buckle as Br is added. Although the Rb–Rb separation is large, ~6.8 Å, focused double and triple MS enabled the determination of the bridging angle. The best fit rms angles, Rb–Br–Rb and Rb–Cl–Rb were $10.5° \pm 1.0°$ and $12.5° \pm 1.0°$, respectively, [45] for $x = 0.55$. In this system at the measurement temperature of 15 K the lattice buckling is dominated by a static distribution of angles since the rms bond angle due to thermal vibration is small, estimated to be only 2.6°.

The polarization-dependence of XAFS permits one to do "crystallography" on anisotropic samples by orienting them in the polarized synchrotron radiation beam [4]. The inclusion of MS improves the ability of surface XAFS to determine the site geometry of adsorbed species, to distinguish between different models for surface reconstruction and to assess the buckling of underlying layers [22,46,47]. It is usually not feasible to perform an unconstrained fit including MS paths to large R, but the distinctiveness of the dominant MS contributions means that simulations can be used to differentiate between different models. This is illustrated with epitaxial growth of Co on Cu (1 1 1) single crystal. Co K-edge XAFS spectra were obtained with the electric vector parallel $E_{\|}$ and perpendicular $E_{\perp}$ to the surface of the Cu substrate to determine if the Co assumed its bulk hcp structure or continued the fcc layering sequence of the Cu substrate [48]. In the fcc structure the fourth shell is enhanced by the focusing effect between the first and fourth neighbours for both $E_{\|}$ and $E_{\perp}$. In the hcp structure focusing is present within the hexagonal planes but is absent for $E_{\perp}$. With the aid of FEFF simulations to the fourth shell films eight monolayers (ML) thick were determined to have a distorted hcp structure. It was established that the first layer of Co continues the stacking of the fcc substrate by growing on the A site for a stacking sequence

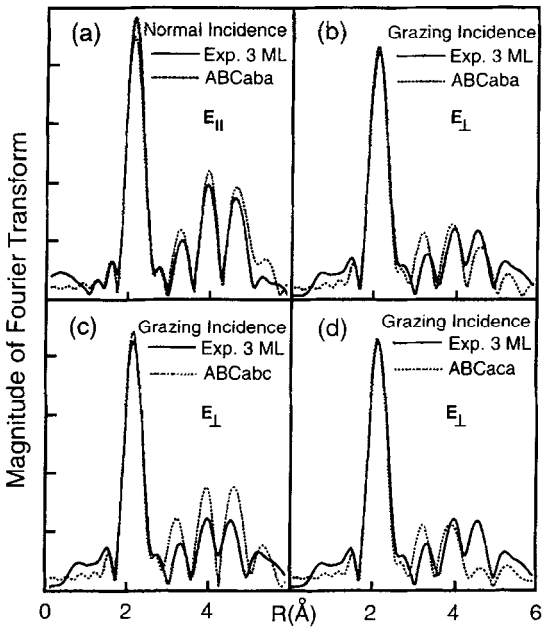

Fig. 6. The magnitude of the Fourier transform (from $k = 3.14$ to 12.66 Å^{-1}) of $k^3\chi(k)$ for three monolayers of Co epitaxially grown on Cu(1 1 1): experiment (solid line) and FEFF6 simulations (dotted line). In Fig. 6(a), the electric vector $\boldsymbol{E}$ is parallel to the Cu surface and in the remaining figures it is perpendicular to the surface. (Taken from Fig. 5 of Ref. [48]).

ABCa where upper case letters denote the substrate and lower case refers to the Co overlayer. Simulations were also used to show that the stacking sequence was ABCaba within the distorted hcp structure. In Fig. 6(a) with $E_{||}$ the agreement is good between simulations and data, independent of stacking sequence. In Figs. 6(b)–(d) the peak positions are well reproduced by the different stacking sequences indicated, but agreement with peak intensities is best for the ABCaba stacking shown in Fig. 6(b).

5. Liquids

In liquids pair distribution functions can be obtained by inverting equations of the form (1). The loss of low k information is a problem since the distribution function is asymmetric. This can be addressed in a model independent way for monatomic disordered systems by the splice method [8] or by fitting to models. But obtaining an accurate first shell coordination number N is difficult since $\int P(r)\,dr$ is determined by the zero-k limit of $k\chi(k)$ (Eq. (1)). It is advantageous to re-express Eq. (1) in terms of the number density and radial distribution function $g(r)$ of liquid state theory (Eq. (60) of Ref. [8]). Then model $g(r)$ can be constructed that satisfy the constraints on $g(r)$ as $r \to \infty$ and on the structure factor $S(0)$ in the thermodynamic limit, $q = 0$ [49]. From the latter condition, Filipponi derived constraint equations on coordination numbers and higher even-order moments of the short range probability density obtained from XAFS and applied them to liquid Pd [49]. Molecular dynamics has also been used to generate partial pair distributions $g_{ij}(r)$ from which a model $\chi(k)$ is constructed. In an iterative process a modified gamma distribution is then used to refine the small r-region of the n–n peak in $g_{ij}(r)$ to improve agreement with the experimental $\chi(k)$. This approach and modifications of it have been used to refine the $g_{ij}(r)$ for liquid metals [50], aqueous and non-aqueous solutions of ions and molecules [29,51]. Its application to determine the coordination geometry of Br ions in methanol is noteworthy for the extensive use of correlation maps to evaluate the errors in the XAFS structural parameters [29].

These calculations used, in part, the GNXAS set of programs in which single and multiple scattering paths are classified according to appropriate *n-body* distribution functions [28]. This permits calculation of the thermal and configuration averages of the *n-body* contributions to the $\chi(k)$ of a model structure with a distribution of displacements. In this treatment it is not necessary to introduce a phenomenological Debye–Waller factor for an average MS path with the atoms in fixed positions [52]. Triangular arrangements of atoms can be specified by a *3-body* distribution function $g_3(R_1,R_2,\theta)$ involving two average distances R_1, R_2 from the X-ray absorbing atom to the scatterers and the angle θ between them. In fitting experimental data, variances in the distances and the angle as well as the bond–bond and bond–angle correlations are included (by a symmetric covariance matrix). In addition to liquids, this approach has been applied to molecules [53], amorphous

Si [54], nanocrystalline Fe [55] and hig-T_C superconductors [56].

XAFS is a fast probe, providing structural information only as long as the core–hole exists, $\sim 10^{-16}$ s and so XAFS measurements provide an ensemble average. In solids the MS formalism has enabled one to determine triangular and higher body correlation functions. The question is: Can the three body (and higher) correlation functions describing the short lived atomic and molecular associations existing in liquids be obtained from XAFS data? In the method of molecular dynamic refinement of $\chi(k)$, the residuals between the experimental and refined model $\chi(k)$ have high frequency components which, although of small amplitude (as in the first shell analysis of Cr discussed above) may be associated with triangular three-body correlations [50]. Additional studies are required.

6. Conclusions

The major experimental and theoretical problems in XAFS spectroscopy have been identified for many years and are now considered to be under control. The signal-to-noise in experimental data has been reduced by improvements in instrumentation and the high flux available at second generation synchrotron radiation sources and will be improved further with third generation sources. The analysis of first shell Gaussian distributions is routine. The problems with anharmonic potentials and asymmetric distributions are understood and can be analysed with different methods. With improvements to background removal procedures it is possible to extract experimental $\chi(k)$ that are reliable to $k_{\min} = 2$ Å^{-1}. Depending upon the degree of disorder and the scatterers involved the upper limit, $k_{\max}$ can exceed 15 Å^{-1}, providing partial pair distributions of high spatial resolution. Comparisons have shown that theoretical scattering amplitudes, phase shifts and inelastic effects can be calculated with sufficient accuracy that the need for experimental reference standards is reduced. There remain uncertainties in the self-energy near the absorption edge and in the magnitude and k-dependence of S_0^2.

Polarization-dependent MS can be included with efficient path-enumeration algorithms so that analysis to 6–8 Å is possible, greatly increasing the power of XAFS as a structural tool. But analysis beyond the nearest neighbour must proceed with caution. Simulations have proven useful in clarifying surface sites and in specifying the layering sequence in epitaxial films. Unconstrained curve-fitting is generally not possible, but, for example, constrained curve-fitting has shown that the crystalline structure of mixed ionic salts is buckled and that antiferrodistortive phase transitions are order–disorder and displacive. Properly treating the dynamical motion of atoms involved in the MS paths remains a problem. Errors in coordination numbers and bond angles are a probable consequence. The loss of low k-data remains a problem in determining the partial pair distributions of liquids, but progress has been made by refining experimental $\chi(k)$ with molecular dynamics.

Acknowledgements

The author wishes to acknowledge useful discussions with A.J. Seary, M.A, Sahiner, D-.T. Jiang, R.A. Gordon and M.K. McManus. This work was supported by the Natural Sciences and Engineering Research Council of Canada. Experiments were performed at SSRL which is supported by the U.S. Department of Energy.

References

[1] T.M. Hayes, J.B. Boyce, in: H. Ehrenreich, F. Seitz, D. Turnbull (Eds.), Solid State Physics, vol. 37, Academic Press, New York, 1982, p. 173.
[2] B.K. Teo, EXAFS: Basic Principles and Data Analysis, Springer, Berlin, 1986.
[3] D.C. Koningsberger, R. Prins (Eds.), X-ray Absorption: Principles, Applications, Techniques of EXAFS, SEXAFS and XANES, Wiley, New York, 1988.
[4] J. Stohr, NEXAFS Spectroscopy, Springer Series in Surface Science: 25, Springer, Berlin, 1992.
[5] D.E Sayers, B.A. Bunker, Ch. 6 in Ref. [3].
[6] E.D. Crozier, Physica B 208&209 (1995) 330.
[7] G. Bunker, Nucl. Instr. and Meth. 207 (1983) 437.
[8] E.D. Crozier, Ch. 9 in Ref. [3].
[9] E.A. Stern, Ch. 1 in Ref. [3].
[10] J. Stohr, Ch. 10 in Ref. [3].

[11] J.C. Mikkelsen, J.B. Boyce, Phys. Rev. Lett. 49 (1982) 1412.
[12] J. Mustre de Leon, S.D. Conradson, I. Batistic, A.R. Bishop, I.D. Raistrick, M.C. Aronson, F.H. Grazon, Phys. Rev. B 45 (1992) 2447.
[13] E.A. Stern, M. Qian, Y. Yacoby, S.M. Heald, M. Maeda, Physica C 209 (1993) 331.
[14] C.H. Booth, F. Bridges, J.B. Boyce, T. Claeson, B.M. Larson, R. Liang, D.A. Bonn, Phys. Rev. B 54 (1996) 9542.
[15] G. Dalba, P. Fornasini, R. Gotter, Phys. Rev. B 52 (1995) 149; G. Dalba, P. Fornasini, F. Rocca, Phys. Rev. B 47 (1993) 8502.
[16] L. Troger, T. Yokohama, D. Arvanitis, T. Leder, M. Tischer, K. Baberschke, Phys. Rev. B 47 (1993) 888.
[17] T. Lederer, D. Arvanitis, G. Comelli, L. Troger, K. Baberschke, Phys. Rev. B 48 (1993); Phys. Rev. B 48 (1993) 11277; T. Yokoyama, H. Hamamatsu, Y. Kitajima, Y. Takata, S. Yagi, T. Ohta, Surf. Sci. 313 (1994) 197.
[18] P.A. Lee, J.B. Pendry, Phys. Rev. B 11 (1975) 2795.
[19] S.I. Zabinsky, J.J. Rehr, A. Ankudinov, R.C. Albers, M.J. Eller, Phys. Rev. B 52 (1995) 2995.
[20] P.J. Durham, J.B. Pendry, C.H. Hodges, Solid State Commun. 38 (1981) 159; D.D. Vvedendsky, D.K. Saldin, J.B. Pendry, Comput. Phys. Commun. 40 (1986) 421.
[21] C. Dagg, L. Troger, D. Arvanitis, K. Baberschke, J. Phys.: Condens. Matter 5 (1993) 6845.
[22] N. Binsted, D. Norman, Phys. Rev. B 22 (1994) 15531.
[23] W. Cook, D.E. Sayers, J. Appl. Phys. 52 (1981) 5024.
[24] G.G. Li, F. Bridges, G. Brown, Phys. Rev. Lett. 68 (1992) 1602.
[25] F. Bridges, C.H. Booth, G.G. Li, Physica B 208&209 (1995) 121.
[26] J.J. Rehr, C.H. Booth, F. Bridges, S.I. Zabinsky, Phys. Rev. B 49 (1994) 12347.
[27] M. Newville, P. Livins, Y. Yacoby, J.J. Rehr, E.A. Stern, Phys. Rev. B 47 (1993) 14126.
[28] A. Filipponi, A. Di Cicco, T.A. Tyson, C.R. Natoli, Solid State Commun. 78 (1991) 265; E. Burratini, P. D'Angelo, A. Di Cicco, A. Filipponi, N.V. Pavel, J. Phys. Chem. 97 (1993) 5486.
[29] P. D'Angelo, A. Di Nola, M. Mangoni, N.V. Pavel, J. Chem. Phys. 104 (1996) 1779.
[30] P. D'Angelo, H.-F. Nolting, N.V. Pavel, Phys. Rev. A. 53 (1996) 798.
[31] P. D'Angelo, A. Di Cicco, A. Filipponi, N.V. Pavel, Phys. Rev. A 47 (1993) 2055.
[32] G.G. Li, F. Bridges, C.H. Booth, Phys. Rev. B 52 (1995) 6332.
[33] Report of the International Workshop on Standards and Criteria in X-ray Absorption Spectroscopy, Phys. B 158 (1989) 701, Eq. (2).
[34] A. Frenkel, E.A. Stern, M. Qian, M. Newville, Phys. Rev. B 48 (1993) 12449.
[35] G.G. Li, F. Bridges, J.B. Boyce, T. Claeson, C. Strom, S.G. Eriksson, S.D. Conradson, Phys. Rev. B 51 (1995) 8564.
[36] B. Houser, R. Ingalls, J.J. Rehr, Physica B 208&209 (1995) 323.
[37] N. Alberding, E.D. Crozier, R. Ingalls, B. Houser, J. De Phys. 47 C8 (1986) 681.
[38] B.K. Teo, J. Am. Chem. Soc. 103 (1981) 3990.
[39] N. Alberding, E.D. Crozier, Phys. Rev. B 27 (1983) 3374.
[40] T. Yokoyama, Y. Yonamoto, T. Ohta, A. Ugawa, Phys. Rev. B 54 (1996) 6921.
[41] B. Rechav, Y. Yacoby, E.A. Stern, J.J. Rehr, M. Newville, Phys. Rev. Lett. 72 (1994) 1352; Physica B 208&209 (1995) 325.
[42] N. Sicron, B. Ravel, Y. Yacoby, E.A. Stern, F. Dogan, J.J. Rehr, Phys. Rev. B 50 (1994) 13168.
[43] Q.T. Islam, B.A. Bunker, Phys. Rev. Lett. 59 (1987) 2701.
[44] A. Frenkel, E.A. Stern, A. Voronel, M. Qian, M. Newville, Phys. Rev. Lett. 71 (1993) 3485.
[45] A.I. Frenkel, E.A. Stern, A. Voronel, S.M. Heald, Solid State Commun. 99 (1996) 67.
[46] D. Arvanitis, K. Babershke, L. Wenzel, Phys. Rev. B 37 (1988) 7143.
[47] J.J. Rehr, Surf. Rev. Lett. 2 (1995) 63.
[48] P. Le Fevre, H. Magnan, O. Heckmann, V. Briois, D. Chandesris, Phys. Rev. B 52 (1995) 11462.
[49] A. Filipponi, J. Phys.: Condens. Matter 6 (1994) 8415.
[50] L. Ottaviano, A. Filipponi, A. Di Cicco, S. Santuci, P. Picozzi, J. Non-Cryst. Solids 156–158 (1993) 112; A. Di Cicco and A. Filipponi, J. Non.-Cryst. Solids 156–158 (1993) 102.
[51] P. D'Angelo, A. Nola, A. Filipponi, N.V. Pavel, D. Roccatano, J. Chem. Phys. 100 (1994) 985.
[52] M. Benfatto, C.R. Natoli, A. Filipponi, Phys. Rev. B 40 (1989) 9626.
[53] A. Filipponi, A. Di Cicco, R. Zanoni, M. Bellatreccia, V. Sessa, C. Dossi, R. Psaro, Chem. Phys. Lett. 184 (1991) 485.
[54] A. Filipponi, A. Di Cicco, M. Benfatto, C.R. Natoli, Europhys. Lett. 13 (1990) 319.
[55] A. Di Cicco, M. Berrettoni, S. Stizza, E. Bonetti, G. Cocco, Phys. Rev. B 50 (1994) 12386.
[56] A. Di Cicco, M. Berrettoni, Phys. Lett. A 176 (1993) 375.